analytical chemistry

pubs.acs.org/ac

Article

Parahydrogen in Reversible Exchange Induces Long-Lived ^{15}N Hyperpolarization of Anticancer Drugs Anastrozole and Letrozole

Keilian MacCulloch,* Austin Browning, Patrick TomHon, Sören Lehmkuhl, Eduard Y. Chekmenev, and Thomas Theis*

Cite This: https://doi.org/10.1021/acs.analchem.2c04817

Read Online

ACCESS | Metrics & More | Article Recommendations | Supporting Information

ABSTRACT: Hyperpolarization modalities overcome the sensitivity limitations of NMR and unlock new applications. Signal amplification by reversible exchange (SABRE) is a particularly cheap, quick, and robust hyperpolarization modality. Here, we employ SABRE for simultaneous chemical exchange of parahydrogen and nitrile-containing anticancer drugs (letrozole or anastrozole) to enhance ^{15}N polarization. Distinct substrates require unique optimal parameter sets, including temperature, magnetic field, or a shaped magnetic field profile. The fine tuning of these parameters for individual substrates is demonstrated here to maximize ^{15}N polarization. After optimization, including the usage of pulsed μT fields, the ^{15}N nuclei on common anticancer drugs, letrozole and anastrozole, can be polarized within 1−2 min. The hyperpolarization can exceed 10%, corresponding to ^{15}N signal enhancement of over 280,000-fold at a clinically relevant magnetic field of 1 T. This sensitivity gain enables polarization studies at naturally abundant ^{15}N enrichment level (0.4%). Moreover, the nitrile ^{15}N sites enable long-lasting polarization storage with $[^{15}N]T_1$ over 9 min, enabling signal detection from a single hyperpolarization cycle for over 30 min.

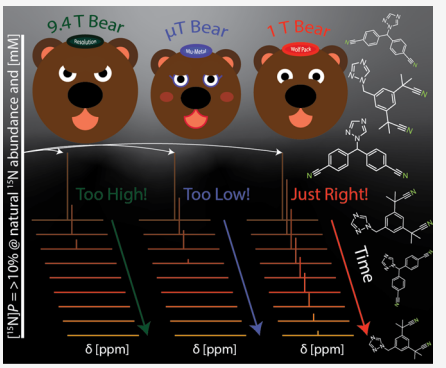

INTRODUCTION

Nuclear magnetic resonance (NMR) is a leading tool for qualifying, quantifying, and monitoring molecules and their dynamics. The advantage of this nondestructive technique stems from the inherent chemical shift resolution afforded by NMR, which offers functional and structural information. However, NMR has inherently low sensitivity compared to other spectroscopic methods. This is because of the minute thermal spin polarization ($<10^{-5}$ at 3 T for ^{15}N), even at high magnetic fields. Hyperpolarization modalities increase the sensitivity of NMR by perturbing thermal spin polarization toward unity. Thus, the increase in signal afforded by hyperpolarization unlocks new doors for more sensitive applications using NMR.

Currently, the dominant hyperpolarization modality employed in tandem with NMR is dynamic nuclear polarization (DNP).[1−10] DNP generates high levels of hyperpolarization on a broad range of substrates, including water, and can directly hyperpolarize site-specific locations on proteins.[11,12] However, in addition to being a lengthy process (on the order of tens of minutes), instrumentation for DNP is expensive (∼1 M), requiring cryogenic temperatures, a superconducting magnet, and high-powered microwave sources.[13] In contrast, signal amplification by reversible exchange (SABRE),[14,15] a para-hydrogen-induced polarization (PHIP) technique,[16−18] can produce hyperpolarized (HP) substrates quickly (∼1 min or less) with little instrumentation cost (∼$20k).

Nonetheless, SABRE often generates lower levels of hyperpolarization and has a more limited substrate scope compared to DNP. Thus, significant effort has been made by the SABRE community to not only optimize the hyperpolarization process for distinct substrate groups but also expand the substrate scope to various biologically relevant molecules.[19,20] Previous work has paved the way for SABRE methods to be employed as a tool for fast, simple, and efficient sensitivity boosters that can readily pair with current analytical methods. For instance, in addition to pioneering ligand−protein studies with DNP, recently, Hilty and colleagues demonstrated the utility of using SABRE for the determination of ligand−protein binding.[21,22] In this work, ligands are first hyperpolarized in methanol. Then, the hyperpolarized solution is mixed with a protein solution at a Y-junction prior to entering an aqueous flow cell. Furthermore, the work from Tessari and colleagues showed the feasibility of detecting amino acids and other metabolites in biological fluids (e.g., urine) using SABRE.[23−25]

Received: October 31, 2022
Accepted: April 24, 2023

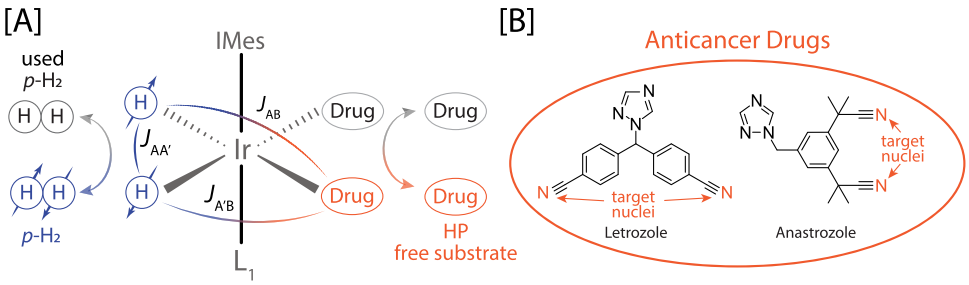

Figure 1. [A] Illustration of parahydrogen and a drug reversibly binding to a transition metal complex forming a temporary *J*-coupling network and [B] the anticancer drugs, letrozole and anastrozole, with target ^{15}N nuclei (at natural isotopic abundance) highlighted in orange.

SABRE utilizes a transition metal catalyst that simultaneously and reversibly binds parahydrogen (p-H_2) and a target substrate. During the SABRE process, a temporary *J*-coupling network forms between the p-H_2 derived hydrides and target nuclei on the substrate. The active SABRE complex and the corresponding *J*-coupling network are illustrated in Figure 1A. Spin order can be transferred to target nuclei through the *J*-coupling network by RF pulses[26−30] or field cycling to low magnetic fields that approach level anticrossings (LACs).[31−33] SABRE efficiency is controlled by exchange rates, *J*-couplings, and Larmor frequencies of the spin system. Therefore, distinct spin systems (different substrates) will have a unique optimal parameter set. Fine tuning of these parameters for individual substrates is instrumental for efficient SABRE hyperpolarization, where the primary key benchmark is the level of attainable polarization, *P* (^{15}N polarization is denoted as [^{15}N] *P* in this document).

A number of FDA-approved drugs have been HP via SABRE, to date, including metronidazole[34−36] ornidazole,[37] nimorazole,[38] pyrazinamide, isoniazid,[39] clotrimazole, fluconazole, voriconazole,[40] and dalfampridine.[41,42] These drugs target hypoxia, tuberculosis, fungal and bacterial infections, and multiple sclerosis. Moreover, they are HP via SABRE using five- or six-membered N-heterocyles rather than the nitrile moiety studied in this work. Here, we utilize SABRE in SHield Enables Alignment Transfer to Heteronuclei (SABRE-SHEATH),[43,44] and coherent SABRE-SEATH using pulsed μT fields, to extend the ^{15}N heteronuclear scope to two bulky, nitrile[45]-containing anticancer drugs, letrozole and anastrozole, as shown in Figure 1B. Both drugs are current generation aromatase inhibitors employed to combat breast cancer[46] and are on the World Health Organization Model List of Essential Medicine, making them highly attractive biological compounds.

Heteronuclei, such as ^{15}N, are attractive hyperpolarization targets because they have virtually no background signal and are associated with long T_1 relaxation times.[19,47] DNP has targeted ^{15}N hyperpolarization since 2000[48,49] and is the most advanced hyperpolarization technique employed for biochemical and biological studies.[50] ^{15}N-choline, for example, has been a model compound for advancing applications of ^{15}N hyperpolarization. In 2008, it was first used in vitro to monitor the phosphorylation of ^{15}N-choline,[49] which is upregulated in cancer metabolism. The first in vivo demonstration of ^{15}N hyperpolarized nuclei was accomplished a couple of years later, where ^{15}N-choline build-up was first detected spectroscopically in a rat brain[51] and later imaged.[52] Further synthetic work improved the lifetime of HP ^{15}N-choline.[53] Other endogenous molecules investigated by DNP include amino acids and carnitine.[54,55] Moreover, Durst and co-workers have also performed a comparison study of HP ^{15}N-enriched glutamine vs HP ^{13}C-enriched urea, where the former was more efficiently localized to areas of interest and was detected over 3 times longer than urea.[56] In addition, ^{15}N-enriched molecules acting as environmental sensors have also been investigated.[57−60] For example, DNP-hyperpolarized ^{15}N-pyridine displayed a remarkable ability to elucidate pH, with over a 90 ppm chemical shift dispersion over 2.1−8.5 pH range.[61] Other notable DNP-hyperpolarized ^{15}N agents include azides and their derivatives[62] as well as nitrate.[63] In addition to DNP studies, both hydrogenative PHIP and nonhydrogenative SABRE demonstrated hyperpolarization of ^{15}N-containing compounds, including choline[64] and other ^{15}N-hyperpolarized markers.[65,66] For a general overview mapping the progress of ^{15}N hyperpolarization using SABRE, we point to review articles in refs 20, 67−69. Based on all this work, we envision the utility of these HP compounds for more sensitive drug screening or as potential exogenous HP contrast agents. Moreover, because aromatase inhibitors (including letrozole and anastrozole studied here) are excreted via urine, we envision that these drugs and the products of their metabolism can potentially be detected in urine samples, paving the way to new applications in the context of cancer management.

Here, we perform hyperpolarization build-up and lifetime studies and then optimize the hyperpolarization process with respect to solution temperature and polarization transfer field (PTF), including pulsed μT fields. At the optimum PTF, the hydride−substrate *J*-coupling is most efficient at transferring spin order from hydrides to substrates. The optimum PTF is dictated by a level anticrossing (LAC) between hydride and substrate spin states. The LAC is established when the hydride−hydride *J*-coupling and the frequency difference between hydride and substrate spins are very close to each other. In the case of hydride-^{15}N systems, like the one studied here, the optimal PTF is typically found at 0.3 μT.

MATERIALS AND METHODS

Chemicals. Letrozole and anastrozole were purchased from Tokyo Chemical Industry Co., Ltd. and Sigma-Aldrich, respectively, and used as delivered. Deuterated methanol was purchased from Cambridge Isotope Laboratories and degassed prior to experimental use. The precatalyst, [Ir(IMes)(COD)-Cl] (IMes = 1,3-bis(2,4,6-trimethylphenyl)imidazol-2-ylidene, COD = 1,5-cyclooctadiene), was synthesized in lab with commercially available starting materials, following a previously published procedure.[70]

Sample Preparation. All samples are prepared using standard Schlenk line conditions, maintaining an oxygen-free environment. Samples are prepared with a 30 mM substrate (letrozole or anastrozole) and a 3 mM precatalyst in 500 μL of

https://doi.org/10.1021/acs.analchem.2c04817
Anal. Chem. XXXX, XXX, XXX−XXX

deuterated methanol. Samples are then transferred into a 7″ medium wall NMR tube (Wilmad 524-PV-7) and connected to our in-house, fully automated, pneumatic shuttling system.[71] Samples are then subjected to 100 psi of parahydrogen, followed by 5 min of bubbling to activate the catalyst prior to experimentation.

Hyperpolarization Build-Up. Samples are first shuttled above the detection field to a polarization transfer field (PTF = 0.3 μT) and are then subjected to bubbling for a distinct time before shuttling back down to a high field (9.4 T) for detection.

Hyperpolarization Lifetime. Samples are first shuttled above the detection field to a polarization transfer field (PTF = 0.3 μT) and are then subjected to 90 s of bubbling. Samples are then stored at a desired field for various times before detection. The PTF and detection field are used as low and high storage fields, respectively, while the fringe field from the detection field is used as an intermediate storage field (∼1 T).

Temperature Dependence. Samples are first heated to a desired temperature in the detection field using the Bruker VT interface. Samples are then shuttled to a PTF (0.3 μT) and are subjected to 90 s of bubbling. Samples are not actively heated while bubbling; thus, the sample experiences light cooling toward room temperature during bubbling. Samples are then shuttled down to the high field for detection.

Static Field Dependence. Samples are shuttled to a desired PTF controlled by a DC power supply and house-built solenoid coil inside mu-metal shields. Samples are then subjected to 90 s of bubbling within the PTF and shuttled down to the high field for detection.

Coherent SHEATH. Samples are shuttled to a dynamic PTF controlled by a DC power supply and home-built solenoid coil inside mu-metal shields. The dynamic PTF alternates between two distinct fields, an "evolution field", denoted Bp, and a "storage field", denoted Bs, for different durations, τ_p and τ_s, respectively, n times for 90 s. The dynamic PTF is generated using a simple circuit board, TTL lines, and solid-state relays. In this method, a pulse sequence can be developed using Bruker software to automate the process. Largest signal enhancements are observed at B_p = 0.5 μT while maintaining a Bs of ∼30 μT, which is the highest achievable field in our experimental design.

RESULTS AND DISCUSSION

The presented series of experimental optimization studies reaches high (>10%) and long-lived ($[^{15}N]T_1$ over 9 min) hyperpolarization on the anticancer drugs at natural isotopic abundance. This work not only broadens the scope of accessible substrates for SABRE-SHEATH but also presents a methodical pathway for hyperpolarizing new SABRE substrates.

In this work, we focused on optimizing the hyperpolarization of chemically symmetric nitrile groups. Although ^{15}N enhancements were observed on the triazole substituent (a triplet peak from the coordinating nitrogen) on both drugs, they were vastly overshadowed by the ^{15}N enhancements observed on the nitrile substituents. In the present chemical system, the nitrile substituents hyperpolarize far more efficiently than the nitrogen-containing heterocycles. First, we studied hyperpolarization build-up and the hyperpolarization lifetime (T_1 constant) for the nitrile substituents on letrozole and anastrozole. We then optimized the hyperpolarization process with respect to solution temperature and PTF. Lastly, we applied a dynamic PTF, referred to as coherent SABRE-SHEATH,[72] to yield maximum hyperpolarization. As the drugs were not isotopically enriched, polarization values were determined using a ^{15}N-enriched pyridine sample thermalized at 9.4 T (see the Supporting Information for more advanced and complete details on $[^{15}N]P$ calculations) following a previously reported method.[43]

Hyperpolarization modalities are often associated with lengthy polarization build-up times that often bottleneck the hyperpolarization process.[73] In SABRE, the polarization build-up time is relatively fast. Accordingly, we first conducted polarization build-up experiments on the nitrile substituents. Letrozole and anastrozole had similar build-up profiles, both reaching a steady state at around 1 min, with ^{15}N T_b (build-up constant) of 21.7 ± 1.4 and 14.6 ± 0.9 s, respectively, as summarized in Table 1. The experimental build-up data were fit using a monoexponential function and are shown together in Figure 2A. For experimental reproducibility, a bubbling time of 90 s was chosen for all succeeding experiments.

Table 1. Hyperpolarization Build-Up and Lifetime Constants for ^{15}N on the Nitrile Substituents of Letrozole and Anastrozole with Errors Given from the Standard Deviation of the Individual Monoexponential Fits

anticancer drug	build-up constant, T_b [s]@0.3 μT	$[^{15}N]T_1$ [s] @9.4 T	$[^{15}N]T_1$ [s]@ 1 T	$[^{15}N]T_1$ [s] @0.3 μT
letrozole	21.7 ± 1.4	9.3 ± 0.1	554.1 ± 12.7	34.7 ± 3.0
anastrozole	14.6 ± 0.9	21.6 ± 0.2	420.8 ± 7.3	27.8 ± 2.9

Long lifetimes of HP states are important for monitoring biological (in vivo) and biochemical processes (in vitro, e.g., protein and drug−protein studies) that have slower or downstream interactions of interest. Previous studies demonstrated that $[^{15}N]T_1$ constants can be extended by storage at an appropriate field.[19,34,40] Often, using a storage field at an intermediate strength (relative to traditional PTFs and detection fields), around 1 T, can significantly extend $[^{15}N]T_1$ times, while noting that the relaxation properties and their field dependencies vary widely depending on the individual molecules and associated spin systems. Thus, in addition to hyperpolarization build-up times, we elucidate hyperpolarization lifetimes at three different fields. Hyperpolarization lifetime studies were investigated at a high field (9.4 T), a low field (0.3 μT), and an intermediate field (1 T).

Agreeing with trends characterized in the literature, short lifetimes are observed at low and high fields, while longer lifetimes are observed at intermediate fields.[19,34,40] At the high field, the $[^{15}N]T_1$ for letrozole and anastrozole was measured to be 9.3 ± 0.1 and 21.6 ± 0.2 s, respectively, as reported in Table 1. These values are slightly lower than the $[^{15}N]T_1$ values at the low field for both letrozole and anastrozole, which were measured to be 34.7 ± 3.0 and 27.8 ± 2.9 s, respectively. Figure 2B shows the remarkably long ^{15}N HP lifetime data recorded at 1 T overlaid with monoexponential fits, yielding $[^{15}N]T_1$ of 554.1 ± 12.7 s (>9 min) and 420.8 ± 7.3 s (>7 min) for letrozole and anastrozole, respectively.

Relaxation at the high field is likely dominated by chemical shift anisotropy (CSA), which scales quadratically with the magnetic field. CSA is mitigated at low fields, which can explain why we observe longer $[^{15}N]T_1$s when transitioning to a low storage field. However, other sources of relaxation become dominant at low field strengths. Specifically, when the

https://doi.org/10.1021/acs.analchem.2c04817
Anal. Chem. XXXX, XXX, XXX−XXX

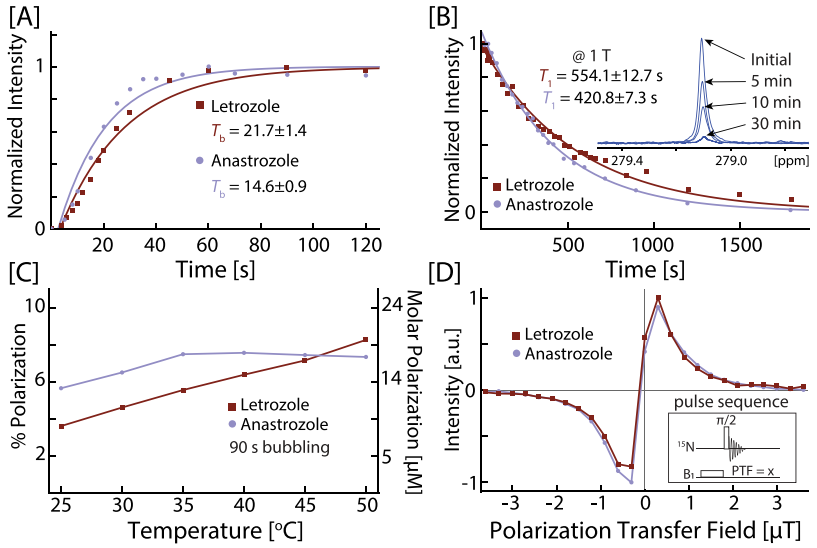

Figure 2. Optimization studies for the nitrile substituent nitrogen on letrozole and anastrozole. [A] Experimental polarization build-up data recorded at 40 °C overlaid with monoexponential fits. [B] Experimental [^{15}N]T_1 data, recorded at 40 °C and stored at 1 T, overlaid with monoexponential fits. [C] Temperature sweep from 25 to 50 °C with 5 °C increments. The polarization is listed on the left axis, while the molar polarization (the product of polarization and spin density) is listed on the right. Experiments were done at natural isotopic abundance (^{15}N is ∼0.4% naturally abundant) using a substrate concentration of 30 mM (see the Materials and Methods Section for more details on sample composition). [D] Static field sweep from 0 to 3.6 μT with 0.3 μT increments with PTFs both parallel (+) and antiparallel (−) to the detection field.

system is not replenished with fresh p-H_2 at 0.3 μT, spin mixing during binding events at low fields leads to relaxation (i.e., the hyperpolarization mechanism is reverted and the hydrides may act as a polarization sink). Evidence supporting this claim is found when comparing the [^{15}N]T_1 of letrozole and anastrozole at the low field. The suspected faster exchanging substrate (experiencing more binding events), anastrozole, has a shorter [^{15}N]T_1 than the slower exchanging substrate (experiencing fewer binding events), letrozole.

At an intermediate field of 1 T, both CSA and spin mixing are mitigated. Instead, dipolar interactions between nuclei become the dominant sources of relaxation,[19] which are weak for the isolated ^{15}N spin in nitriles. Nitrogen on a nitrile lacks nearby spin 1/2 nuclei that could induce strong dipolar relaxation. Thus, mitigating high- and low-field relaxation sources and selecting an isolated target nucleus give rise to an exceptional environment for magnetization storage. Other methods used to extend T_1s have been shown in the literature, for example, isotopic labeling where protons are replaced for deuterium[47] or the usage of long-lived singlet states.[74]

In addition to relaxation parameters, another critical parameter in SABRE is the exchange rate on the SABRE complex. The chemical exchange of p-H_2 and a target substrate need to be similar to the frequency of spin order transfer, governed by the temporary J-coupling network on the active SABRE catalyst, for efficient spin transfer.

There are several methods reported in the literature that have been used to control the exchange of both p-H_2 and a target substrate. These methods consist of either increasing or decreasing the electronic density on the metal center or by increasing or decreasing the steric crowding around the metal center.[75,76] These strategies not only allow for more efficient spin order transfer but also enable the hyperpolarization of new substrates. The work led by Duckett and colleagues demonstrated that SABRE can be used to hyperpolarize α-keto acids and nitrites by modulating exchange with the incorporation of a cosubstrate.[77,78] In addition to the referenced strategies, direct heating or cooling can be used to modulate exchange rates.[40,79] Following these findings, a temperature sweep was performed on both target drugs. We chose to sweep from room temperature (25 °C) to 50 °C with 5 °C increments, shown in Figure 2C, to shed light on the exchange dynamics.

Prominently, we observed an increase in polarization as the temperature was increased. Letrozole reaches maximum hyperpolarization at 50 °C (limited by experimental setup), while anastrozole reaches a maximum at 40 °C but levels off at further elevated temperatures. The difference in observed maxima is likely due to the chemical environment around the nitrile substituents on both drugs. Anastrozole has additional steric bulk close to the nitrile substituent compared to letrozole, likely leading to faster exchange. Therefore, the faster exchanging substrate, anastrozole, will be expected to reach maximum hyperpolarization at lower temperatures relative to the faster exchanging substrate, letrozole. We note that the substrate exchange rate also controls the hydride exchange rate, as we have shown with ab initio calculations[80] because hydride exchange does require substrate exchange events for monodentate ligands. These findings not only support that temperature modulation represents a key hyperpolarization parameter but also additionally suggest that relative exchange rates can be unveiled through HP temperature studies.

In traditional SABRE-SHEATH experiments, the sample is subjected to a very low (<1 μT) static PTF. At sub μT fields, LACs between coupled spin states arise. At a LAC, spin mixing is most efficient, aiding in polarization build-up.[31,43] For this reason, we investigated the μT regime to unveil the most efficient PTF. We swept from 0 to 3 μT with 0.3 μT increments with static PTFs aligned parallel (+) and antiparallel (−) to the detection field, as shown in Figure

https://doi.org/10.1021/acs.analchem.2c04817
Anal. Chem. XXXX, XXX, XXX−XXX

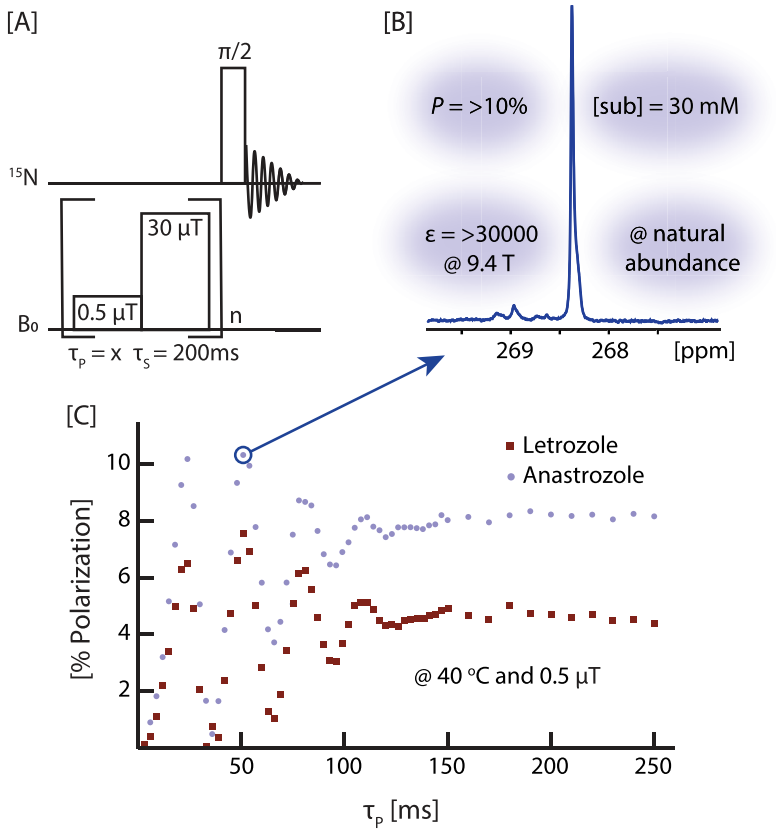

Figure 3. [A] Graphical representation of coherent SABRE-SHEATH pulse sequence, [B] NMR signal of anastrozole when τ_P = 51 ms, and [C] applying coherent SABRE-SHEATH pulse sequence sweeping from τp = 0 to τp = 250 ms while keeping B_P, B_S, and τ_P constant (B_P = 0.5 μT, B_S = 30 μT and τ_S = 200 ms).

2D. Hyperpolarization was most efficiently generated at ±0.3 μT for both drugs.

However, recent advances reported in the literature demonstrate that a static field only generates a fraction of the hyperpolarization of a dynamic pulse (field).[81−84] The referenced work has shown significant boosts in hyperpolarization by applying shaped PTFs to the sample during polarization build-up in a variety of distinct patterns.[81−84] On this notion, we implemented a previously published pulse sequence referred to as coherent SABRE-SHEATH, originally used by Lindale et al., to increase hyperpolarization on acetonitrile (chemically similar to the nitrile substituents on letrozole and anastrozole).[72]

Coherent SABRE-SHEATH first evolves spin order using an efficient PTF, B_P, for a short time, τ_P, and then quickly switches to an elevated storage field, B_S, where little to no evolution is expected, for a lengthier duration, τ_S, that is preoptimized (see the Supporting Information for τ_S optimization) to allow fresh p-H_2 to associate with the catalyst. A graphical representation of the pulse sequence is shown in Figure 3A. A plot sweeping through discrete τ_P values, while B_P, B_S, and τ_P remain constant, is shown in Figure 3C for both letrozole and anastrozole.

Notably, the pulse sequence drives higher polarization than what can be generated using a static field. Both compounds reach maximum enhancements when τ_P = 51 ms. For anastrozole, the maximum enhancement corresponds to [^{15}N]P over 10% (at natural isotopic abundance and mM concentration) and the corresponding spectrum is shown in Figure 3B. The boost in [^{15}N]P is due to more efficient spin order transfer generated by turning the usually incoherent spin order transfer into a coherently driven, unidirectional mechanism. In addition to boosting the hyperpolarization level, the coherent SABRE-SHEATH data of Figure 3B also elucidates the hyperpolarization transfer dynamics.

In conclusion, this work demonstrates a systematic optimization study for nitrile moieties of two bulky anticancer drugs achieving high degrees of [^{15}N]P with long HP state lifetimes.

First, the polarization build-up was investigated for both letrozole and anastrozole. Both anticancer drugs had similar build-up constants, reaching a [^{15}N]P steady state in ∼1 min. For comparison, DNP has a build-up time on the order of tens of minutes to an hour.[13] Additionally, by exploring a clinically relevant field of 1 T, we were able to achieve [^{15}N]T_1 constants of ∼9 and ∼7 min on letrozole and anastrozole, respectively. Next, we explored exchange dynamics of the SABRE system by modulating the solution temperature and swept through the μT regime to elucidate the optimal PTF. Maximum enhancements were measured at 50 °C for letrozole and 40 °C for anastrozole, corresponding to [^{15}N]P of 8.3 and 7.6%, respectively, at the experimental optimal PTF of 0.3 μT. We also showed that controlling the solution temperature, in a small window (25 °C), can more than double the net [^{15}N]P. Finally, we pushed the hyperpolarization to over 10% on anastrozole (at natural isotopic abundance and mM concen-

https://doi.org/10.1021/acs.analchem.2c04817
Anal. Chem. XXXX, XXX, XXX−XXX

tration) by applying coherent SABRE-SHEATH, showing the importance of exploring nonstatic fields.

There are still limitations in the presented work inhibiting direct translation to applications such as drug screening. For instance, the substrate concentrations investigated here are relatively high and are currently limited to nonaqueous conditions. However, the feasibility of studying SABRE hyperpolarization at natural abundance of ^{15}N substantially streamlines the experimental workflow and potentially enables the screening of many other nitrile-containing drugs, biomolecules, etc. We envision that once a lead compound is identified, additional sensitivity gains can be obtained via ^{15}N-labeling to perform binding studies at relevant concentrations. There are also ongoing efforts in the field to develop biocompatible formulations of SABRE-hyperpolarized compounds in aqueous media[85−90]—we hope future developments in this area will mitigate the current limitations.

■ ASSOCIATED CONTENT

Supporting Information

The Supporting Information is available free of charge at https://pubs.acs.org/doi/10.1021/acs.analchem.2c04817.

Single ^{15}N scan of pure ^{15}N-enriched pyridine thermalized at 9.4 T used for polarization calculations; single ^{1}H scan of concentrated toluene in CD_3OD without (blue) and with (red) capillary; τ_P duration sweep from 50−500 ms with 50 ms increments. (PDF)

■ AUTHOR INFORMATION

Corresponding Authors

Keilian MacCulloch − *Department of Chemistry, North Carolina State University, Raleigh, North Carolina 27606, United States;* orcid.org/0000-0002-4506-5057; Email: kjmaccul@ncsu.edu

Thomas Theis − *Department of Chemistry, North Carolina State University, Raleigh, North Carolina 27606, United States; Joint Department of Biomedical Engineering, University of North Carolina, Chapel Hill and North Carolina State University, Raleigh, North Carolina 27606, United States; Department of Physics, North Carolina State University, Raleigh, North Carolina 27606, United States;* orcid.org/0000-0001-6779-9978; Email: ttheis@ncsu.edu

Authors

Austin Browning − *Department of Chemistry, North Carolina State University, Raleigh, North Carolina 27606, United States*

Patrick TomHon − *Department of Chemistry, North Carolina State University, Raleigh, North Carolina 27606, United States;* orcid.org/0000-0003-3202-9812

Sören Lehmkuhl − *Department of Chemistry, North Carolina State University, Raleigh, North Carolina 27606, United States;* orcid.org/0000-0002-1321-7677

Eduard Y. Chekmenev − *Department of Chemistry, Wayne State University, Detroit, Michigan 48202, United States; Integrative Biosciences (Ibio), Wayne State University, Karmanos Cancer Institute (KCI), Detroit, Michigan 48202, United States; Russian Academy of Sciences, 119991 Moscow, Russia;* orcid.org/0000-0002-8745-8801

Complete contact information is available at: https://pubs.acs.org/10.1021/acs.analchem.2c04817

Notes

The authors declare the following competing financial interest(s): Thomas Theis and Patrick TomHon hold stock in Vizma Life Sciences LLC (VLS) and T.T. is President of VLS. VLS is developing products related to the research being reported. The terms of this arrangement have been reviewed and approved by NC State University in accordance with its policy on objectivity in research. Eduard Y. Chekmenev discloses a stake of ownership in XeUS Technologies, LTD. E.Y. Chekmenev is a member of the Scientific Advisory Board of VLS.

The authors declare the following competing financial interest(s): T.T. and P.T. hold stock in Vizma Life Sciences (VLS). P.T. is a senior engineer at V.L.S., and T.T. is the president of V.L.S. V.L.S. is developing products related to the research being reported. The terms of this arrangement have been reviewed and approved by NC State University in accordance with its policy on objectivity in research. E.Y.C. discloses a stake of ownership in XeUS Technologies, Ltd.

■ ACKNOWLEDGMENTS

Research reported in this publication was supported by the National Institute of Biomedical Imaging and Bioengineering of the National Institutes of Health under Award Nos. NIH R21EB025313 and NIH R01EB029829. The content is solely the responsibility of the authors and does not necessarily represent the official views of the National Institutes of Health. In addition, the authors acknowledge funding from the Mallinckrodt Foundation, the National Science Foundation under Award No. NSF CHE-1904780 from the National Cancer Institute under Award No. NCI 1R21CA220137, and from the North Carolina Biotechnology Center in the form of a Translational Research Grant. Finally, they would like to acknowledge the support from NCSU's METRIC providing access to NMR instrumentation.

■ REFERENCES

(1) Stern, Q.; Milani, J.; Vuichoud, B.; Bornet, A.; Gossert, A. D.; Bodenhausen, G.; Jannin, S. *J. Phys. Chem. Lett.* **2015**, *6*, 1674−1678.

(2) Wang, Y.; Hilty, C. *Anal. Chem.* **2020**, *92*, 13718−13723.

(3) Min, H.; Sekar, G.; Hilty, C. *ChemMedChem* **2015**, *10*, 1559−1563.

(4) Kim, Y.; Hilty, C.Applications of Dissolution-DNP for NMR Screening. In *Methods in Enzymology*; Elsevier, 2019; Vol. *615*, pp 501−526.

(5) Keshari, K. R.; Kurhanewicz, J.; MacDonald, J. M.; Wilson, D. M. *Analyst* **2012**, *137*, 3427−3429.

(6) Kress, T.; Walrant, A.; Bodenhausen, G.; Kurzbach, D. *J. Phys. Chem. Lett.* **2019**, *10*, 1523−1529.

(7) Buratto, R.; Bornet, A.; Milani, J.; Mammoli, D.; Vuichoud, B.; Salvi, N.; Singh, M.; Laguerre, A.; Passemard, S.; Gerber-Lemaire, S.; Jannin, S.; Bodenhausen, G. *ChemMedChem* **2014**, *9*, 2509−2515.

(8) Hu, J.; Kim, J.; Hilty, C. *J. Phys. Chem. Lett* **2022**, *13*, 3819−3823.

(9) Kim, Y.; Liu, M.; Hilty, C. *Anal. Chem.* **2016**, *88*, 11178−11183.

(10) Wang, Y.; Kim, J.; Hilty, C. *Chem. Sci.* **2020**, *11*, 5935−5943.

(11) Gauto, D.; Dakhlaoui, O.; Marin-Montesinos, I.; Hediger, S.; De Paëpe, G. *Chem. Sci.* **2021**, *12*, 6223−6237.

(12) Hilty, C.; Kurzbach, D.; Frydman, L. *Nat. Protoc.* **2022**, *17*, 1621−1657.

(13) Pinon, A. C.; Capozzi, A.; Ardenkjær-Larsen, J. H. *Magn. Reson. Mater. Phys., Biol. Med.* **2021**, *34*, 5−23.

(14) Adams, R. W.; Duckett, S. B.; Green, R. A.; Williamson, D. C.; Green, G. G. R. *J. Chem. Phys.* **2009**, *131*, No. 194505.

(15) Adams, R. W.; Aguilar, J. A.; Atkinson, K. D.; Cowley, M. J.; Elliott, P. I. P.; Duckett, S. B.; Green, G. G. R.; Khazal, I. G.; Lopez-Serrano, J.; Williamson, D. C. *Science* **2009**, *323*, 1708−1711.
(16) Bowers, C. R.; Weitekamp, D. P. *Phys. Rev. Lett.* **1986**, *57*, 2645−2648.
(17) Bowers, C. R.; Weitekamp, D. P. *J. Am. Chem. Soc.* **1987**, *109*, 5541−5542.
(18) Eisenschmid, T. C.; Kirss, R. U.; Deutsch, P. P.; Hommeltoft, S. I.; Eisenberg, R.; Bargon, J.; Lawler, R. G.; Balch, A. L. *J. Am. Chem. Soc.* **1987**, *109*, 8089−8091.
(19) Colell, J. F. P.; Logan, A. W. J.; Zhou, Z.; Shchepin, R. V.; Barskiy, D. A.; Ortiz, G. X.; Wang, Q.; Malcolmson, S. J.; Chekmenev, E. Y.; Warren, W. S.; Theis, T. *J. Phys. Chem. C* **2017**, *121*, 6626−6634.
(20) Barskiy, D. A.; Knecht, S.; Yurkovskaya, A. V.; Ivanov, K. L. *Prog. Nucl. Magn. Reson. Spectrosc.* **2019**, *114*−*115*, 33−70.
(21) Mandal, R.; Pham, P.; Hilty, C. *Chem. Sci.* **2021**, *12*, 12950−12958.
(22) Mandal, R.; Pham, P.; Hilty, C. *Anal. Chem.* **2022**, *94*, 11375−11381.
(23) Reile, I.; Eshuis, N.; Hermkens, N. K. J.; Van Weerdenburg, B. J. A.; Feiters, M. C.; Rutjes, F. P. J. T.; Tessari, M. *Analyst* **2016**, *141*, 4001−4005.
(24) Sellies, L.; Aspers, R. L. E. G.; Feiters, M. C.; Rutjes, F. P. J. T.; Tessari, M. *Angew. Chem., Int. Ed.* **2021**, *60*, 26954−26959.
(25) Fraser, R.; Rutjes, F. P. J. T.; Feiters, M. C.; Tessari, M. *Acc. Chem. Res.* **2022**, *55*, 1832−1844.
(26) Roy, S. S.; Stevanato, G.; Rayner, P. J.; Duckett, S. B. *J. Magn. Reson.* **2017**, *285*, 55−60.
(27) Theis, T.; Truong, M.; Coffey, A. M.; Chekmenev, E. Y.; Warren, W. S. *J. Magn. Reson.* **2014**, *248*, 23−26.
(28) Lindale, J. R.; Eriksson, S. L.; Warren, W. S. *Phys. Chem. Chem. Phys.* **2022**, *24*, 7214−7223.
(29) Theis, T.; Feng, Y.; Wu, T.; Warren, W. S. *J. Chem. Phys.* **2014**, *140*, No. 014201.
(30) Pravdivtsev, A. N.; Yurkovskaya, A. V.; Vieth, H. M.; Ivanov, K. L. *Phys. Chem. Chem. Phys.* **2014**, *16*, 24672−24675.
(31) Ivanov, K. L.; Yurkovskaya, A. V.; Vieth, H. M. *J. Chem. Phys.* **2008**, *128*, No. 154701.
(32) Pravdivtsev, A. N.; Yurkovskaya, A. V.; Kaptein, R.; Miesel, K.; Vieth, H. M.; Ivanov, K. L. *Phys. Chem. Chem. Phys.* **2013**, *15*, 14660−14669.
(33) Pravdivtsev, A. N.; Yurkovskaya, A. V.; Vieth, H. M.; Ivanov, K. L.; Kaptein, R. *ChemPhysChem* **2013**, *14*, 3327−3331.
(34) Kiryutin, A. S.; Yurkovskaya, A. V.; Ivanov, K. L. *ChemPhysChem* **2021**, *22*, 1470−1477.
(35) Barskiy, D. A.; Shchepin, R. V.; Coffey, A. M.; Theis, T.; Warren, W. S.; Goodson, B. M.; Chekmenev, E. Y. *J. Am. Chem. Soc.* **2016**, *138*, 8080−8083.
(36) Shchepin, R. V.; Birchall, J. R.; Chukanov, N. V.; Kovtunov, K. V.; Koptyug, I. V.; Theis, T.; Warren, W. S.; Gelovani, J. G.; Goodson, B. M.; Shokouhi, S.; Rosen, M. S.; Yen, Y. F.; Pham, W.; Chekmenev, E. Y. *Chem. - Eur. J.* **2019**, *25*, 8829−8836.
(37) Iali, W.; Moustafa, G. A. I.; Dagys, L.; Roy, S. S. *Magn. Reson. Chem.* **2021**, *59*, 1199−1207.
(38) Salnikov, O. G.; Chukanov, N. V.; Svyatova, A.; Trofimov, I. A.; Kabir, M. S. H.; Gelovani, J. G.; Kovtunov, K. V.; Koptyug, I. V.; Chekmenev, E. Y. *Angew. Chem., Int. Ed.* **2021**, *60*, 2406−2413.
(39) Zeng, H.; Xu, J.; Gillen, J.; McMahon, M. T.; Artemov, D.; Tyburn, J. M.; Lohman, J. A. B.; Mewis, R. E.; Atkinson, K. D.; Green, G. G. R.; Duckett, S. B.; van Zijl, P. C. M. *J. Magn. Reson.* **2013**, *237*, 73−78.
(40) MacCulloch, K.; Tomhon, P.; Browning, A.; Akeroyd, E.; Lehmkuhl, S.; Chekmenev, E. Y.; Theis, T. *Magn. Reson. Chem.* **2021**, *59*, 1225−1235.
(41) Skovpin, I. V.; Svyatova, A.; Chukanov, N.; Chekmenev, E. Y.; Kovtunov, K. V.; Koptyug, I. V. *Chem. - Eur. J.* **2019**, *25*, 12694−12697.
(42) Chukanov, N. V.; Salnikov, O. G.; Trofimov, I. A.; Kabir, M. S. H.; Kovtunov, K. V.; Koptyug, I. V.; Chekmenev, E. Y. *ChemPhysChem* **2021**, *22*, 960−967.
(43) Theis, T.; Truong, M. L.; Coffey, A. M.; Shchepin, R. V.; Waddell, K. W.; Shi, F.; Goodson, B. M.; Warren, W. S.; Chekmenev, E. Y. *J. Am. Chem. Soc.* **2015**, *137*, 1404−1407.
(44) Truong, M. L.; Theis, T.; Coffey, A. M.; Shchepin, R. V.; Waddell, K. W.; Shi, F.; Goodson, B. M.; Warren, W. S.; Chekmenev, E. Y. *J. Phys. Chem. C* **2015**, *119*, 8786−8797.
(45) Mewis, R. E.; Green, R. A.; Cockett, M. C. R.; Cowley, M. J.; Duckett, S. B.; Green, G. G. R.; John, R. O.; Rayner, P. J.; Williamson, D. C. *J. Phys. Chem. B* **2015**, *119*, 1416−1424.
(46) Buzdar, A. U.; Robertson, J. F. R.; Eiermann, W.; Nabholtz, J. M. *Cancer* **2002**, *95*, 2006−2016.
(47) Nonaka, H.; Hirano, M.; Imakura, Y.; Takakusagi, Y.; Ichikawa, K.; Sando, S. *Sci. Rep.* **2017**, *7*, No. 40104.
(48) Sarkar, R.; Comment, A.; Vasos, P. R.; Jannin, S.; Gruetter, R.; Bodenhausen, G.; Hall, H.; Kirik, D.; Denisov, V. P. *J. Am. Chem. Soc.* **2009**, *131*, 16014−16015.
(49) Gabellieri, C.; Reynolds, S.; Lavie, A.; Payne, G. S.; Leach, M. O.; Eykyn, T. R. *J. Am. Chem. Soc.* **2008**, *130*, 4598−4599.
(50) Ardenkjaer-Larsen, J.-H.; Boebinger, G. S.; Comment, A.; Duckett, S.; Edison, A. S.; Engelke, F.; Griesinger, C.; Griffin, R. G.; Hilty, C.; Maeda, H.; Parigi, G.; Prisner, T.; Ravera, E.; van Bentum, J.; Vega, S.; Webb, A.; Luchinat, C.; Schwalbe, H.; Frydman, L. *Angew. Chem.* **2015**, *127*, 9292−9317.
(51) Cudalbu, C.; Comment, A.; Kurdzesau, F.; van Heeswijk, R. B.; Uffmann, K.; Jannin, S.; Denisov, V.; Kirike, D.; Gruetter, R. *Phys. Chem. Chem. Phys.* **2010**, *12*, 5818−5823.
(52) Friesen-Waldner, L. J.; Wade, T. P.; Thind, K.; Chen, A. P.; Gomori, J. M.; Sosna, J.; McKenzie, C. A.; Katz-Brull, R. *J. Magn. Reson. Imaging* **2015**, *41*, 917−923.
(53) Kumagai, K.; Kawashima, K.; Akakabe, M.; Tsuda, M.; Abe, T.; Tsuda, M. *Tetrahedron* **2013**, *69*, 3896−3900.
(54) Chiavazza, E.; Viale, A.; Karlsson, M.; Aime, S. *Contrast Media Mol. Imaging* **2013**, *8*, 417−421.
(55) Morze, C.; Engelbach, J. A.; Reed, G. D.; Chen, A. P.; Quirk, J. D.; Blazey, T.; Mahar, R.; Malloy, C. R.; Garbow, J. R.; Merritt, M. E. *Magn. Reson. Med.* **2021**, *85*, 1814−1820.
(56) Durst, M.; Chiavazza, E.; Haase, A.; Aime, S.; Schwaiger, M.; Schulte, R. F. *Magn. Reson. Med.* **2016**, *76*, 1900−1904.
(57) Nonaka, H.; Hata, R.; Doura, T.; Nishihara, T.; Kumagai, K.; Akakabe, M.; Tsuda, M.; Ichikawa, K.; Sando, S. *Nat. Commun.* **2013**, *4*, No. 2411.
(58) Suh, E. H.; Kovacs, Z. *ACS Phys. Chem. Au* **2022**, *3*, 167−171.
(59) Hata, R.; Nonaka, H.; Takakusagi, Y.; Ichikawa, K.; Sando, S. *Chem. Commun.* **2015**, *51*, 12290−12292.
(60) Suh, E. H.; Park, J. M.; Lumata, L.; Sherry, A. D.; Kovacs, Z. *Commun. Chem.* **2020**, *3*, No. 185.
(61) Jiang, W.; Lumata, L.; Chen, W.; Zhang, S.; Kovacs, Z.; Sherry, A. D.; Khemtong, C. *Sci. Rep.* **2015**, *5*, No. 9104.
(62) Bae, J.; Zhang, G.; Park, H.; Warren, W. S.; Wang, Q. *Chem. Sci.* **2021**, *12*, 14309−14315.
(63) Gamliel, A.; Uppala, S.; Sapir, G.; Harris, T.; Nardi-Schreiber, A.; Shaul, D.; Sosna, J.; Gomori, J. M.; Katz-Brull, R. *J. Magn. Reson.* **2019**, *299*, 188−195.
(64) Reineri, F.; Viale, A.; Ellena, S.; Alberti, D.; Boi, T.; Giovenzana, G. B.; Gobetto, R.; Premkumar, S. S. D.; Aime, S. *J. Am. Chem. Soc.* **2012**, *134*, 11146−11152.
(65) McCormick, J.; Korchak, S.; Mamone, S.; Ertas, Y. N.; Liu, Z.; Verlinsky, L.; Wagner, S.; Glöggler, S.; Bouchard, L. S. *Angew. Chem., Int. Ed.* **2018**, *57*, 10692−10696.
(66) Bales, L. B.; Kovtunov, K. V.; Barskiy, D. A.; Shchepin, R. V.; Coffey, A. M.; Kovtunova, L. M.; Bukhtiyarov, A. V.; Feldman, M. A.; Bukhtiyarov, V. I.; Chekmenev, E. Y.; Koptyug, I. V.; Goodson, B. M. *J. Phys. Chem. C* **2017**, *121*, 15304−15309.
(67) Hövener, J.; Pravdivtsev, A. N.; Kidd, B.; Bowers, C. R.; Glöggler, S.; Kovtunov, Kv.; Plaumann, M.; Katz-Brull, R.; Buckenmaier, K.; Jerschow, A.; Reineri, F.; Theis, T.; Shchepin,

https://doi.org/10.1021/acs.analchem.2c04817
Anal. Chem. XXXX, XXX, XXX−XXX

Rv.; Wagner, S.; Bhattacharya, P.; Zacharias, N. M.; Chekmenev, E. Y. *Angew. Chem.* **2018**, *130*, 11310−11333.
(68) Park, H.; Wang, Q. *Chem. Sci.* **2022**, *13*, 7378−7391.
(69) Rayner, P. J.; Duckett, S. B. *Angew. Chem.* **2018**, *130*, 6854−6866.
(70) Vázquez-Serrano, L. D.; Owens, B. T.; Buriak, J. M. *Chem. Commun.* **2002**, *21*, 2518−2519.
(71) TomHon, P.; Akeroyd, E.; Lehmkuhl, S.; Chekmenev, E. Y.; Theis, T. *J. Magn. Reson.* **2020**, *312*, No. 106700.
(72) Lindale, J. R.; Eriksson, S. L.; Tanner, C. P. N.; Zhou, Z.; Colell, J. F. P.; Zhang, G.; Bae, J.; Chekmenev, E. Y.; Theis, T.; Warren, W. S. *Nat. Commun.* **2019**, *10*, No. 395.
(73) Nikolaou, P.; Goodson, B. M.; Chekmenev, E. Y. *Chem. - Eur. J.* **2015**, *21*, 3156−3166.
(74) Theis, T.; Ortiz, G. X.; Logan, A. W. J.; Claytor, K. E.; Feng, Y.; Huhn, W. P.; Blum, V.; Malcolmson, S. J.; Chekmenev, E. Y.; Wang, Q.; Warren, W. S. *Sci. Adv.* **2016**, *2*, No. e1501438.
(75) Fekete, M.; Ahwal, F.; Duckett, S. B. *J. Phys. Chem. B* **2020**, *124*, 4573−4580.
(76) Colell, J. F. P.; Logan, A. W. J.; Zhou, Z.; Lindale, J. R.; Laasner, R.; Shchepin, R. V.; Chekmenev, E. Y.; Blum, V.; Warren, W. S.; Malcolmson, S. J.; Theis, T. *Chem. Commun.* **2020**, *56*, 9336−9339.
(77) Tickner, B. J.; Semenova, O.; Iali, W.; Rayner, P. J.; Whitwood, A. C.; Duckett, S. B. *Catal. Sci. Technol.* **2020**, *10*, 1343−1355.
(78) Rayner, P. J.; Fekete, M.; Gater, C. A.; Ahwal, F.; Turner, N.; Kennerley, A. J.; Duckett, S. B. *J. Am. Chem. Soc.* **2022**, *144*, 8756−8769.
(79) Tomhon, P.; Abdulmojeed, M.; Adelabu, I.; Nantogma, S.; Kabir, M. S. H.; Lehmkuhl, S.; Chekmenev, E. Y.; Theis, T. *J. Am. Chem. Soc.* **2022**, *144*, 282−287.
(80) Lin, K.; TomHon, P.; Lehmkuhl, S.; Laasner, R.; Theis, T.; Blum, V. *ChemPhysChem* **2021**, *22*, 1947−1957.
(81) Pravdivtsev, A. N.; Kempf, N.; Plaumann, M.; Bernarding, J.; Scheffler, K.; Hövener, J. B.; Buckenmaier, K. *ChemPhysChem* **2021**, *22*, 2381−2386.
(82) Dagys, L.; Bengs, C.; Levitt, M. H. *J. Chem. Phys.* **2021**, *155*, No. 154201.
(83) Li, X.; Lindale, J. R.; Eriksson, S. L.; Warren, W. S. *Phys. Chem. Chem. Phys.* **2022**, *24*, 16462−16470.
(84) Eriksson, S. L.; Lindale, J. R.; Li, X.; Warren, W. S. *Sci. Adv.* **2022**, *8*, No. eabl3708.
(85) Schmidt, A. B.; De Maissin, H.; Adelabu, I.; Nantogma, S.; Ettedgui, J.; Tomhon, P.; Goodson, B. M.; Theis, T.; Chekmenev, E. Y. *ACS Sens.* **2022**, *7*, 3430−3439.
(86) Shi, F.; He, P.; Best, Q. A.; Groome, K.; Truong, M. L.; Coffey, A. M.; Zimay, G.; Shchepin, R. V.; Waddell, K. W.; Chekmenev, E. Y.; Goodson, B. M. *J. Phys. Chem. C* **2016**, *120*, 12149−12156.
(87) Truong, M. L.; Shi, F.; He, P.; Yuan, B.; Plunkett, K. N.; Coffey, A. M.; Shchepin, R. V.; Barskiy, D. A.; Kovtunov, K. V.; Koptyug, I. V.; Waddell, K. W.; Goodson, B. M.; Chekmenev, E. Y. *J. Phys. Chem. B* **2014**, *118*, 13882−13889.
(88) Hövener, J. B.; Schwaderlapp, N.; Borowiak, R.; Lickert, T.; Duckett, S. B.; Mewis, R. E.; Adams, R. W.; Burns, M. J.; Highton, L. A. R.; Green, G. G. R.; Olaru, A.; Hennig, J.; Von Elverfeldt, D. *Anal. Chem.* **2014**, *86*, 1767−1774.
(89) Browning, A.; Mcculloch, K.; Bedoya, D. G.; Dedesma, C.; Goodson, B. M.; Rosen, M. S.; Chekmenev, E. Y.; Yen, Y.-F.; Tomhon, P.; Theis, T. Facile Hyperpolarization Chemistry for Molecular Imaging and Metabolic Tracking of [1-13 C]Pyruvate in Vivo *ChemRxiv* 2023.
(90) Colell, J. F. P.; Emondts, M.; Logan, A. W. J.; Shen, K.; Bae, J.; Shchepin, R. V.; Ortiz, G. X.; Spannring, P.; Wang, Q.; Malcolmson, S. J.; Chekmenev, E. Y.; Feiters, M. C.; Rutjes, F. P. J. T.; Blümich, B.; Theis, T.; Warren, W. S. *J. Am. Chem. Soc.* **2017**, *139*, 7761−7767.

https://doi.org/10.1021/acs.analchem.2c04817
Anal. Chem. XXXX, XXX, XXX−XXX